RFI Mitigation for UWB Radar Via Hyperparameter-Free Sparse SPICE Methods

Jiaying Ren, Tianyi Zhang, Jian Li, *Fellow, IEEE*, Lam H. Nguyen, and Petre Stoica, *Fellow, IEEE*

***Abstract*— Radio frequency interference (RFI) causes serious problems to ultrawideband (UWB) radar operations due to severely degrading radar imaging capability and target detection performance. This paper formulates proper data models and proposes novel methods for effective RFI mitigation. We first apply the single-snapshot Sparse Iterative Covariance-based Estimation (SPICE) algorithm to data from each pulse repetition interval for RFI mitigation and discuss the connection of SPICE to the l_1-penalized least absolute deviation (l_1-PLAD) approach. Then, we devise a modified group SPICE algorithm and we prove that it is equivalent to a special case of the $l_{1,2}$-PLAD method. The modified group SPICE algorithm can be applied to data from a coherent processing interval for effective RFI mitigation. Both the single-snapshot SPICE and the modified group SPICE methods simultaneously exploit the sparsity properties of both RFI spectrum and UWB radar target echoes. Unlike the existing sparsity-based RFI suppression methods, such as the robust principal component analysis algorithm, the proposed methods are hyperparameter-free and therefore easier to use in practical applications. Furthermore, the fast implementation of the SPICE methods is considered by exploiting the special structures of both single-snapshot and multiple-snapshot covariance matrices. Finally, the results obtained from applying the SPICE methods to simulated data as well as measured data collected by the U.S. Army Research Laboratory synthetic aperture radar system are presented to demonstrate the effectiveness of the proposed methods.**

***Index Terms*— Radio frequency interference (RFI) mitigation, ultrawideband synthetic aperture radar (UWB SAR), Sparse Iterative Covariance-based Estimation (SPICE), $l_{1,q}$-penalized least absolute deviation ($l_{1,q}$-PLAD).**

I. Introduction

ULTRAWIDEBAND (UWB) radar operating at frequencies from under 100 MHz to several gigahertz has been used in a wide range of applications, such as for ground penetration and through-the-wall sensing, because of its penetration and high range resolution capabilities [1]–[5]. In recent years, as the radio frequency spectrum becomes highly congested, the received radar signals are increasingly corrupted by radio frequency interferences (RFIs). Typical RFI sources include the AM/FM radios, TV stations, cellular phones, and other radiation devices whose operating frequency bands overlap with the UWB radar signal spectrum [6]. These RFI signals pose a significant hindrance to UWB radar operations causing reduced signal-to-noise ratio (SNR) and degraded radar imaging quality. Therefore, it is necessary to effectively suppress the RFI signals from the observed UWB radar data before imaging and target detection.

RFI mitigation in UWB radar systems is a challenging problem since the RFI signals are difficult to predict and hard to model accurately due to their dynamic range and diverse modulation schemes. Several methods have been developed for RFI mitigation, including RFI suppression via filtering techniques [6]–[11] and RFI extraction based on interference estimation [12]–[16]. The former suppression approaches, such as notch filtering, subband filtering, and adaptive filtering, although popular due to their simplicity, usually suffer from high sidelobe levels and target energy loss problems [6]–[11]. The latter class of RFI extraction methods consists of techniques based on, for example, parametric modeling [12], spectral decomposition [13], eigensubspace decompositions [14], [16], and independent component analysis (ICA) [15], [16]. They are known to provide satisfactory performance under certain assumptions. However, in the case of severe RFI, the required assumptions are no longer valid, leading to inaccurate RFI estimation and insufficient RFI extraction. For instance, eigensubspace decomposition [14], [16] and ICA [15], [16] have difficulties in distinguishing between RFI sources and UWB radar echoes when they have similar power levels within the same subspace.

Recently, RFI mitigation methods based on sparse or low-rank recovery methodologies have been introduced in [17]–[24]. The sparse recovery approach solves the RFI problem by modeling both the desired UWB radar echo signal and the RFI sources as sparse with respect to well-designed dictionaries [17]–[19]. This approach works well if the data model is accurate but suffers from the drawback that an additional step of dictionary learning is required. In [20] and [21], a joint sparse and low-rank model for RFI mitigation is exploited. Compared to the original approach in [17]–[19], this improved method eliminates the need for any specific prior knowledge about the interference through taking advantage of

Manuscript received July 31, 2018; accepted October 9, 2018. Date of publication December 5, 2018; date of current version May 28, 2019. This work was supported in part by the U.S. Army Research Laboratory and the U.S. Army Research Office under Grant W911NF-16-2-0223, in part by the National Science Foundation under Grant 1704240, and in part by the Swedish Research Council. *(Corresponding author: Jian Li.)*

J. Ren, T. Zhang, and J. Li are with the Department of Electrical and Computer Engineering, University of Florida, Gainesville, FL 32611 USA (e-mail: jiaying.ren@ufl.edu; tianyi.zhang@ufl.edu; li@dsp.ufl.edu).

L. H. Nguyen is with the Army Research Laboratory, Adelphi, MD 20783-1138 USA (e-mail: lam.h.nguyen2.civ@mail.mil).

P. Stoica is with the Department of Information Technology, Uppsala University, SE-751 05 Uppsala, Sweden (e-mail: ps@it.uu.se).

Color versions of one or more of the figures in this paper are available online at http://ieeexplore.ieee.org.

Digital Object Identifier 10.1109/TGRS.2018.2880758

the low-rank property of RFI. The latest algorithms mitigate the RFI problem by using the robust principal component analysis (RPCA) approach that exploits the low-rank structure of the RFI spectrum and the sparsity properties of the UWB radar echoes. These algorithms can be used to blindly separate the RFI signals and UWB radar echo signals from the observed data without needing any prior information on the RFI [22]–[24]. However, all these sparse and low-rank-based algorithms require a fine-tuning of one or more hyperparameters, and this parameter tuning is not a simple task in practical applications due to lack of prior information on the RFI and radar signals.

The SParse Iterative Covariance-based Estimation (SPICE) algorithm is a sparse semiparametric technique proposed for spectral analysis and array processing using one or more snapshots [25], [26]. Unlike the parametric methods, SPICE circumvents the requirement of model order determination via exploiting a nonparametric data model as well as the sparsity property of the solution. SPICE is based on a covariance fitting criterion and does not require the selection of any user parameters. In [27]–[30], the single-snapshot SPICE algorithm is shown to be equivalent to the l_1-penalized least absolute deviation (l_1-PLAD) approach [31] and the square-root least absolute shrinkage and selection operator (SR-LASSO) method [32] (for a particular choice of the hyperparameter) under the assumption of heteroscedastic noise and homoscedastic noise, respectively. In particular, this means that the single-snapshot SPICE algorithm provides an appropriate choice of the hyperparameter for l_1-PLAD and SR-LASSO. In [26], a multiple-snapshot SPICE is obtained by extending the single-snapshot SPICE algorithm and the extended method is shown to be related to a weighted $l_{1,2}$-norm minimization problem. In [33], the group version of SPICE, referred to as group SPICE, is proposed via relaxing the covariance fitting criterion for the group-sparse estimation problem. The group SPICE algorithm can be regarded as a special case of the group variants of l_1-PLAD (i.e., $l_{1,q}$-PLAD ($1 \leq q \leq 2$)) or SR-LASSO for two different noise cases. In sum, we have a host of SPICE algorithms, but it is not clear how they can be used for enhanced RFI mitigation in UWB radar systems.

This paper proposes a novel framework for hyperparameter-free RFI mitigation based on the SPICE approaches [25]–[29], [33]. Our main contributions can be summarized as follows.

1) For RFI mitigation based on a single-pulse repetition interval (PRI), we formulate a proper data model to exploit the sparsity properties of the fast-time RFI spectrum as well as the UWB radar echo signals in the fast-time domain. The single-snapshot SPICE algorithm [25], which is equivalent to a special case of l_1-PLAD, is shown to be a good choice, based on this data model, for extracting the RFI sources from the observed RFI-contaminated signal without the need for selecting any user parameter.

2) For improved RFI mitigation, we formulate a proper data model across multiple PRIs that belong to a coherent processing interval (CPI), to exploit the row-sparsity structure of the RFI spectrum and model the UWB radar echo signals as sparse impulses in the fast-time domain of each PRI. Then, based on this data model, we devise a modified group SPICE algorithm for multiple-PRI-based RFI mitigation, which is shown to be equivalent to a special case of $l_{1,2}$-PLAD under the heteroscedastic noise condition.

3) We propose fast implementations of the SPICE algorithms by using the conjugate gradient least squares (CGLS) approach [34], [35] and the fast Fourier transform (FFT) to reduce the computational burden of the proposed RFI mitigation procedure. We also provide a fast computation method for the group SPICE algorithms.

4) Both simulated and experimental results are presented to confirm the effectiveness of the proposed RFI mitigation methods under various operating conditions including the presence of strong RFI sources.

5) We demonstrate, using both simulated and experimentally measured data, that the proposed methods outperform existing UWB radar RFI mitigation methods. Our techniques are applicable directly in the raw sample domain and do not require any restrictive prior information and assumptions, nor the selection of any user parameters. Hence, the proposed methods can be utilized in a preprocessing and denoising step for raw radar signals to effectively suppress RFI signals, prior to other signal processing and imaging steps.

The rest of this paper is organized as follows. In Section II, we formulate the single-PRI-based RFI mitigation problem and discuss how to solve this problem by using the single-snapshot SPICE algorithm. Next, in Section III, we formulate the multiple-PRI-based RFI mitigation problem and derive the proposed modified group SPICE algorithm. In Section IV, we consider fast implementations of the aforementioned SPICE methods. Finally, in Section V, we provide simulated and experimental results that confirm the validity of the proposed RFI mitigation methods for UWB radar systems.

Notation: We denote the vectors and matrices by boldface lowercase and uppercase letters, respectively. $(\cdot)^T$ denotes the transpose operation, $(\cdot)^*$ denotes the conjugate transpose operation, vec$(\cdot)$ denotes the vectorization operation, diag$(\cdot)$ denotes the diagonalization operation, and $\bigotimes$ denotes the Kronecker product. $\mathbf{x}_{k\cdot}$ and $\mathbf{x}_{\cdot k}$ refer to the kth row and kth column of matrix $\mathbf{X}$, respectively, and $x_{i,j}$ refers to the (i, j)th element of $\mathbf{X}$. $\mathbf{R} \in \mathbb{C}^{N\times M}$ denotes a complex-valued $N \times M$ matrix. $|\cdot|$ denotes the magnitude of a scalar. $\|\cdot\|_p$ is the symbol used for the l_p-norm of a vector or the entrywise l_p-norm of a matrix, $\|\cdot\|_F$ is the Frobenius norm of a matrix, and $\|\cdot\|_{1,q}$, which is defined as $\|\mathbf{X}\|_{1,q} = \sum_{k=1}^{K} \|\mathbf{x}_{k\cdot}\|_q$, denotes the $l_{1,q}$ norm of a matrix. $\mathbf{I}_N$ denotes the $N \times N$ identity matrix. If $\mathbf{P} = \text{diag}([p_1, \ldots, p_K])$ is a diagonal matrix, the square root of $\mathbf{P}$ is defined as $\mathbf{P}^{1/2} = \text{diag}([p_1^{1/2}, \ldots, p_K^{1/2}])$. Finally, $\mathbf{x} \succeq 0$ means that every element of $\mathbf{x}$ is greater than or equal to 0.

Reproducibility: The MATLAB codes used to produce the numerical illustrations of this paper can be downloaded from http://www.sal.ufl.edu/code.html.

II. Single-PRI-Based RFI Mitigation

In this section, we show how the single-snapshot SPICE algorithm [25] can be used to separate and extract the RFI

signals from the RFI-contaminated data within a single PRI. We first formulate a single-PRI data model for the UWB radar system. Then, we show that an l_1-PLAD optimization metric is an appropriate semiparametric choice to mitigate the RFI problem by exploiting the sparsity property of the fast-time RFI spectrum as well as the desired UWB radar echo signals in the fast-time domain. Finally, we consider the single-snapshot SPICE algorithm, which provides a useful selection of the user parameter for l_1-PLAD [25], and show how the hyperparameter-free single-snapshot SPICE algorithm can be utilized to solve the RFI mitigation problem effectively.

A. Problem Statement

Consider a data vector from an impulse UWB radar system consisting of N samples per PRI, referred to as the N fast-time samples, which are contaminated by RFI and noise. We model the observed complex-valued radar data vector, $\mathbf{y} \in \mathbb{C}^N$, as follows:

$$\mathbf{y} = \begin{bmatrix} \mathbf{a}_1 & \cdots & \mathbf{a}_K \end{bmatrix} \begin{bmatrix} x_1 \\ \vdots \\ x_K \end{bmatrix} + \mathbf{s} + \boldsymbol{\gamma} = \mathbf{B}\mathbf{x} + \mathbf{s} + \boldsymbol{\gamma} \quad (1)$$

with $\mathbf{Bx}$ denoting the RFI sources, $\mathbf{s}$ is the desired UWB radar echoes, and $\boldsymbol{\gamma}$ is the disturbance. Furthermore, $\{\mathbf{a}_k\}_{k=1}^K$ is a set of Fourier vectors:

$$\mathbf{a}_k = \begin{bmatrix} 1 & \cdots & e^{\mathrm{j}2\pi f_k(N-1)} \end{bmatrix}^T \quad (2)$$

corresponding to the normalized frequencies $\{f_k\}_{k=1}^K$, which form a grid covering the interval $[-0.5, 0.5]$. We assume that this grid is fine enough and that the frequencies (normalized by the sampling frequency) corresponding to the RFI sources are on this grid (or practically, close to points on the grid). Thus, $\mathbf{x}$ can be interpreted as the unknown fast-time spectrum of the RFI sources. In case of severe RFI contaminations, $\mathbf{Bx}$ can be much stronger than $\mathbf{s}$. Our goal is to estimate $\mathbf{s}$ from the observed data $\mathbf{y}$ to achieve RFI mitigation. Note that the actual number of the frequency components in the RFI is unknown, and usually is much smaller than the number of grid points K. We will exploit this sparsity property of $\mathbf{x}$ below for effective RFI mitigation.

There are two main observations that we can use for RFI removal: 1) the desired UWB radar echo signal vector $\mathbf{s}$ is sparse in the fast-time domain and 2) the RFI spectrum $\mathbf{x}$ is sparse in the frequency domain. The sparse nature of the UWB radar echoes has been observed and utilized by the proposers of recent RFI mitigation algorithms [22]–[24]. Fig. 1 presents a typical example showing that the UWB impulse radar echoes within a PRI, which were measured by the U.S. Army Research Laboratory (ARL) radar in the absence of RFI, are quite sparse. Note that this sparsity property is also valid for UWB stepped-frequency or chirp radar systems since the echoes received by these radar systems can be easily converted into narrow sparse pulses through pulse compression. The sparsity of the RFI spectrum $\mathbf{x}$ is illustrated in Fig. 2, where the fast-time RFI spectrum from a single PRI, also measured by the ARL radar, is depicted. RFI sources, such as the AM/FM radios, digital TV, and cellular phones, tend to have their

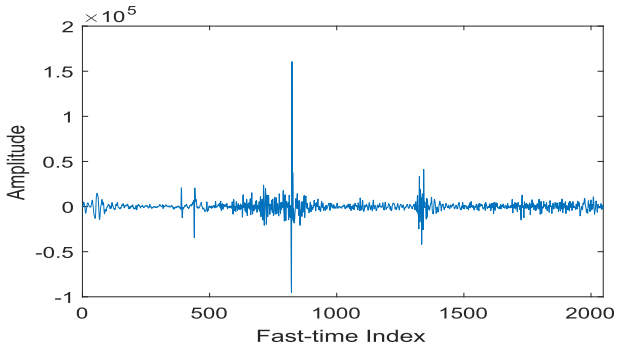

Fig. 1. Example of measured ARL UWB impulse radar echo signal in the fast-time domain, within a single PRI.

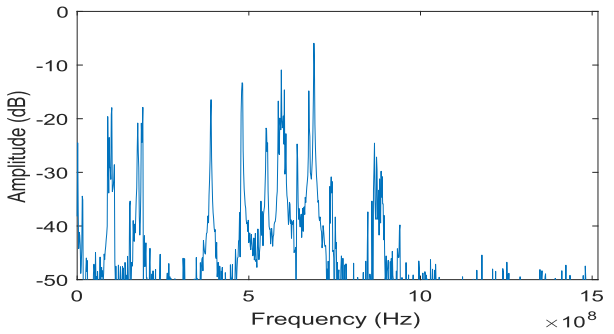

Fig. 2. Example of the fast-time RFI spectrum within one PRI for the measured data collected by the experimental ARL radar receiver.

power concentrated in a small number of narrow frequency bands resulting in a sparse spectrum in the fast-time frequency domain, whereas the full frequency band of the UWB radar system is occupied by the radar echoes.

B. l_1-PLAD Formulation

To utilize the sparsity properties of the RFI spectrum and the UWB radar echoes in the fast-time domain for RFI mitigation from receiver measurements, we propose the following l_1-PLAD approach:

$$\min_{\mathbf{x}} \|\mathbf{y} - \mathbf{B}\mathbf{x}\|_1 + \lambda \|\mathbf{x}\|_1 \quad (3)$$

where $\mathbf{e} = \mathbf{y} - \mathbf{Bx}$ comprises the sparse UWB radar signal vector $\mathbf{s}$ and noise vector $\boldsymbol{\gamma}$. $\|\cdot\|_1$ represents the l_1-norm, which is a sparsity-enforcing metric, and λ is a hyperparameter used to balance the two objectives of enforcing sparsity on both $\mathbf{e}$ and $\mathbf{x}$. The tuning of λ is required to achieve a satisfactory performance in practice. However, the selection of λ is by no means a simple task in practical applications due to lack of prior information on $\mathbf{s}$ and $\mathbf{x}$.

C. Single-Snapshot SPICE

To deal with the hyperparameter selection problem of l_1-PLAD, we consider the single-snapshot SPICE algorithm [25], which is shown to be equivalent to the l_1-PLAD approach (for a particular choice of the hyperparameter) under the assumption of heteroscedastic noise [27], [28].

Single-snapshot SPICE is a data-adaptive and user-parameter-free approach first proposed for single-snapshot spectral analysis and array processing [25]. The main idea of this algorithm is to iteratively minimize a covariance fitting criterion [25], as briefly explained below. SPICE postulates the following covariance matrix model for $\mathbf{y}$:

$$\mathbf{R} = E(\mathbf{y}\mathbf{y}^*) = \mathbf{A}\mathbf{P}\mathbf{A}^* \tag{4}$$

where

$$\mathbf{A} \triangleq [\mathbf{B}\ \mathbf{I}_N] = [\mathbf{a}_1 \cdots \mathbf{a}_K \mathbf{a}_{K+1} \cdots \mathbf{a}_{K+N}] \tag{5}$$

$$\mathbf{P} \triangleq \text{diag}([p_1 \cdots p_{K+N}]) \tag{6}$$

with $\mathbf{a}_{K+i}$ denoting the ith column of $\mathbf{I}_N$, and $\{p_k\}_{k=1}^{K}$ and $\{p_k\}_{k=K+1}^{K+N}$ denoting the unknown powers of $\mathbf{x}$ and unknown noise powers, respectively. It is worth mentioning that this covariance matrix model holds under the assumption that the RFI amplitudes $\{x_i\}_{i=1}^{K}$ as well as the elements of $\mathbf{e}$ are uncorrelated. However, it has been shown in the literature that the SPICE algorithms are insensitive to this assumption [25], [26], [33], which can, in fact, be viewed as a prior model for $\mathbf{R}$ rather than a real assumption. Note that the elements of $\mathbf{e}$, which is regarded as the noise vector in the SPICE algorithm, are allowed to have different powers, and hence, we consider the heteroscedastic noise case here.

The SPICE estimate of $\{p_k\}_{k=1}^{K+N}$ is obtained by minimizing the covariance fitting criterion [25]

$$\|\mathbf{R}^{-1/2}(\mathbf{y}\mathbf{y}^* - \mathbf{R})\|_F^2 \tag{7}$$

or equivalently

$$\min_{\{p_k \geq 0\}} \mathbf{y}^*\mathbf{R}^{-1}\mathbf{y} + \sum_{k=1}^{K+N} w_k p_k \tag{8}$$

where $w_k = (\|\mathbf{a}_k\|_2^2 / \|\mathbf{y}\|_2^2)$. Because the above-mentioned optimization problem is convex, the global estimate of $\{p_k\}_{k=1}^{K+N}$ can be obtained, for instance, by the iterative algorithm of [25] and [27]

$$\widehat{p}_k^{j+1} = \widehat{p}_k^{j} |\mathbf{a}_k^* \widehat{\mathbf{R}}_j^{-1} \mathbf{y}| / \sqrt{w_k} \tag{9}$$

where j denotes the iteration index, $k = 1, \ldots, K+N$, and $\widehat{\mathbf{R}}_j = \mathbf{A}\widehat{\mathbf{P}}_j\mathbf{A}^*$. In addition, the linear minimum mean-squared estimate (LMMSE) $\{\widehat{x}_k\}_{k=1}^{K}$ of $\{x_k\}_{k=1}^{K}$, based on $\{\widehat{p}_k\}_{k=1}^{K}$, is given by [27]

$$\widehat{x}_k = \widehat{p}_k \mathbf{a}_k^* \widehat{\mathbf{R}}^{-1} \mathbf{y}, \quad \text{for } k = 1, \cdots, K \tag{10}$$

where $\widehat{\mathbf{R}} = \mathbf{A}\widehat{\mathbf{P}}\mathbf{A}^*$.

The single-snapshot SPICE algorithm together with the LMMSE estimator is a special case of the l_1-PLAD in (3) with $\lambda = \sqrt{N}$ [27], [28]. Therefore, the single-snapshot SPICE algorithm provides not only a useful choice of λ in (3) but also an efficient implementation of the l_1-PLAD. We initialize the single-snapshot SPICE algorithm with the power estimates obtained using the periodogram method (see [36]). We obtain an estimate $\widehat{\mathbf{x}}$ of the RFI spectrum $\mathbf{x}$ by using (9) and (10). Finally, the recovered radar echo signal $\widehat{\mathbf{s}}$ is given by $\widehat{\mathbf{s}} = \mathbf{y} - \mathbf{B}\widehat{\mathbf{x}}$.

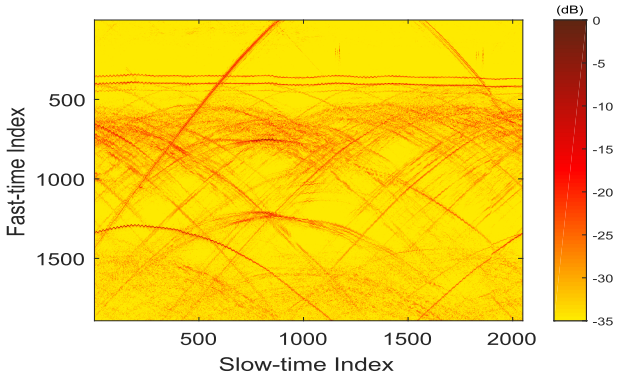

Fig. 3. Example of the measured ARL UWB impulse radar signal within a CPI.

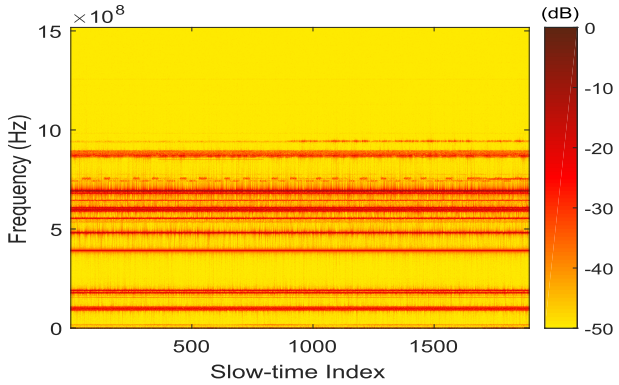

Fig. 4. Example of fast-time RFI spectrum versus PRI (or slow-time index) for the RFI data measured by the ARL radar receiver.

III. Multiple-PRI-Based RFI Mitigation

In this section, we consider RFI mitigation using data within a CPI consisting of M PRIs. The PRI index is also referred to as the slow-time index. We first formulate a multiple-PRI-based RFI mitigation data model. We then show how an $l_{1,2}$-PLAD approach can be used to exploit the row-sparsity of the RFI spectrum matrix and the element-sparsity of the UWB radar echo matrix. Then, we review the multiple-snapshot SPICE algorithm [26] and explore its relationship with $l_{1,2}$-PLAD. Then, we present a sparse-plus-group-sparse data model for the RFI-contaminated signal and consider using the group SPICE algorithm [33] for RFI mitigation. Finally, we devise a modified group SPICE algorithm, which is equivalent to a special case of $l_{1,2}$-PLAD, to achieve hyperparameter-free RFI mitigation in the multiple PRIs case. When the frequencies of the RFI sources change only slightly over the CPI, multiple-PRI-based RFI mitigation may yield improved performance compared to its single-PRI-based counterpart.

A. Problem Statement and $l_{1,2}$-PLAD Formulation

The M RFI-contaminated UWB radar data vectors within a CPI are collected into a matrix as follows:

$$\mathbf{Y} = \mathbf{B}\mathbf{X} + \mathbf{S} + \mathbf{\Gamma}. \tag{11}$$

The column $\mathbf{y}_{\cdot m}$ of $\mathbf{Y} \in \mathbb{C}^{N\times M}$ denotes the mth PRI data vector of the N received fast-time samples consisting of the RFI $\mathbf{Bx}_{\cdot m}$, the desired UWB radar signal $\mathbf{s}_{\cdot m}$, and the disturbances $\boldsymbol{\gamma}_{\cdot m}$, $m = 1, \ldots, M$. As discussed in Section II, each column of $\mathbf{X}$ is referred to as the unknown fast-time spectrum of the RFI for the corresponding PRI.

We model the desired UWB radar signal $\mathbf{S}$ as element-sparse [22]–[24] and the RFI spectrum matrix $\mathbf{X}$ as row-sparse. Fig. 3 demonstrates the element-sparsity of a typical UWB radar echo matrix $\mathbf{S}$ collected by the ARL radar in the absence of RFI. Fig. 4 shows that the RFI spectrum matrix $\mathbf{X}$ collected by the ARL radar receiver indeed exhibits row-sparsity within the CPI. Our goal is to separate the UWB radar signal $\mathbf{S}$ from the RFI $\mathbf{BX}$ by exploiting the aforementioned sparsity properties of $\mathbf{S}$ and $\mathbf{X}$.

A natural choice for extracting $\mathbf{BX}$ from the collected data matrix $\mathbf{Y}$ is the following $l_{1,2}$-PLAD approach:

$$\min_{\mathbf{X}} \|\mathbf{Y} - \mathbf{BX}\|_1 + \lambda \|\mathbf{X}\|_{1,2}. \tag{12}$$

As before, $\mathbf{E} = \mathbf{Y} - \mathbf{BX}$ is composed of the desired UWB radar signal and noise, and λ is a user parameter that balances the tradeoff between the two components of the criterion in (12). Similar to the l_1-PLAD optimization problem, the selection of λ in (12) is a difficult task in practical applications. In order to circumvent this selection problem, we will analyze and exploit the relationships between the $l_{1,2}$-PLAD metric and various versions of the SPICE metric, as explained in the following sections.

B. Multiple-Snapshot SPICE

Inspired by the relationship between single-snapshot SPICE and l_1-PLAD [27], [28], we consider below the connection between multiple-snapshot SPICE [26] and $l_{1,2}$-PLAD. Let $\widehat{\mathbf{R}}$ denote the sample covariance matrix for the multiple-snapshot case

$$\widehat{\mathbf{R}} = \frac{\mathbf{Y}\mathbf{Y}^*}{M}. \tag{13}$$

The multiple-snapshot SPICE algorithm minimizes the following covariance fitting criterion [25], [26]

$$\|\mathbf{R}^{-1/2}(\widehat{\mathbf{R}} - \mathbf{R})\|_F^2 \tag{14}$$

or equivalently

$$\min_{\{p_k \geq 0\}} \operatorname{tr}(\widehat{\mathbf{R}}\mathbf{R}^{-1}\widehat{\mathbf{R}}) + \sum_{k=1}^{K+N} w_k p_k \tag{15}$$

where $w_k = \|\mathbf{a}_k\|_2^2$. Let $\mathbf{A} = [\mathbf{B} \ \ \mathbf{I}_N]$, as before. The multiple-snapshot SPICE problem can be reformulated as the following weighted $l_{1,2}$-norm minimization problem with respect to a matrix $\mathbf{C} \in \mathbb{C}^{(K+N)\times N}$

$$\min_{\mathbf{C}} \sum_{k=1}^{K+N} {w_k}^{1/2} \|\mathbf{c}_{k\cdot}\|_2, \quad \text{s.t. } \mathbf{AC} = \widehat{\mathbf{R}}. \tag{16}$$

Once the optimal solution $\mathbf{C}$ to the above-mentioned problem is obtained, $\{p_k\}_{k=1}^{K+N}$ can be retrieved from $\mathbf{C}$ [26].

It is proven in Appendix B that, for $M \geq N$ and full-rank $\widehat{\mathbf{R}}$, any matrix $\mathbf{C}$ that satisfies the constraint in (16) must have the following general form:

$$\mathbf{C} = \begin{bmatrix} \mathbf{X} \\ \mathbf{Y} - \mathbf{BX} \end{bmatrix} \frac{\mathbf{Y}^*}{M}. \tag{17}$$

Inserting (17) into (16) yields an equivalent optimization problem to the multiple-snapshot SPICE

$$\min_{\mathbf{X}} \|(\mathbf{Y} - \mathbf{BX})\mathbf{Y}^*\|_{1,2} + \sqrt{\mathbf{N}}\|\mathbf{X}\mathbf{Y}^*\|_{1,2}. \tag{18}$$

Since (18) is quite different from the proposed $l_{1,2}$-PLAD in (12), the multiple-snapshot SPICE is not considered to be a good candidate for RFI mitigation.

C. Group SPICE

Next, the group SPICE algorithm [33] is considered, which is a generalization of SPICE for enforcing the group sparsity. The connection between group SPICE and group variants of l_1-PLAD, i.e., $l_{1,q}$-PLAD, $(1 \leq q \leq 2)$, has been established in [33]. To apply group SPICE to RFI mitigation, we first rewrite the signal model (11) into a sparse-plus-group-sparse version

$$\widetilde{\mathbf{y}} = \widetilde{\mathbf{B}}\widetilde{\mathbf{x}} + \widetilde{\mathbf{e}} \tag{19}$$

where

$$\widetilde{\mathbf{y}} = \operatorname{vec}(\mathbf{Y}) = [\mathbf{y}_{\cdot 1}{}^T \cdots \mathbf{y}_{\cdot M}{}^T]^T \in \mathbb{C}^{NM} \tag{20}$$

$$\widetilde{\mathbf{e}} = \operatorname{vec}(\mathbf{E}) = [\mathbf{e}_{\cdot 1}{}^T \cdots \mathbf{e}_{\cdot M}{}^T]^T \in \mathbb{C}^{NM} \tag{21}$$

$$\widetilde{\mathbf{x}} = [\,\mathbf{x}_{1\cdot} \quad \cdots \quad \mathbf{x}_{K\cdot}\,]^T \in \mathbb{C}^{KM} \tag{22}$$

and $\widetilde{\mathbf{B}} \in \mathbb{C}^{NM\times KM}$ can be expressed as

$$\begin{aligned} \widetilde{\mathbf{B}} &= \begin{bmatrix} \mathbf{a_1} & \mathbf{0} & \cdots & \mathbf{0} & \mathbf{a}_K & \mathbf{0} & \cdots & \mathbf{0} \\ \mathbf{0} & \mathbf{a_1} & \cdots & \mathbf{0} & \mathbf{0} & \mathbf{a}_K & \cdots & \mathbf{0} \\ \vdots & \vdots & \ddots & \vdots & \vdots & \vdots & \ddots & \vdots \\ \mathbf{0} & \mathbf{0} & \cdots & \mathbf{a_1} & \mathbf{0} & \mathbf{0} & \cdots & \mathbf{a}_K \end{bmatrix} \\ &= \begin{bmatrix} \widetilde{\mathbf{a}}_{11} & \widetilde{\mathbf{a}}_{12} & \cdots & \widetilde{\mathbf{a}}_{1M} & \cdots & \widetilde{\mathbf{a}}_{K1} & \widetilde{\mathbf{a}}_{K2} & \cdots & \widetilde{\mathbf{a}}_{KM} \end{bmatrix}. \end{aligned} \tag{23}$$

To verify (23), note that $\operatorname{vec}(\mathbf{BX}) = \operatorname{vec}(\sum_{k=1}^{K} \mathbf{a}_k \mathbf{x}_{k\cdot}) = \sum_{k=1}^{K} (\mathbf{I}_M \bigotimes \mathbf{a}_k)\mathbf{x}_{k\cdot}^T = \widetilde{\mathbf{B}}\widetilde{\mathbf{x}}$.

Since $\widetilde{\mathbf{x}}$ is composed of K groups and the group $\mathbf{x}_{k\cdot}$ corresponds to the kth row of $\mathbf{X}$, the use of $\widetilde{\mathbf{x}}$ makes a group sparsity formulation of the RFI spectrum $\mathbf{X}$ possible. In addition, it is clear that $\widetilde{\mathbf{e}}$ can be regarded as a sparse noise vector. Hence, group SPICE can be used to obtain $\widehat{\widetilde{\mathbf{x}}}$ from the vectorized observations $\widetilde{\mathbf{y}}$ via minimizing a special covariance fitting criterion [33].

The covariance matrix of $\widetilde{\mathbf{y}}$ is defined similar to (4)

$$\mathbf{R}_{\mathrm{g}} = E(\widetilde{\mathbf{y}}\widetilde{\mathbf{y}}^*) = \widetilde{\mathbf{A}}\widetilde{\mathbf{P}}\widetilde{\mathbf{A}}^* \tag{24}$$

where

$$\widetilde{\mathbf{A}} = \left[\widetilde{\mathbf{B}}\ \mathbf{I}_{NM}\right] = \left[\ \mathbf{A}_1 \ \cdots \ \mathbf{A}_K \ \ \widetilde{\mathbf{a}}_{K+1} \cdots \widetilde{\mathbf{a}}_{K+NM}\ \right] \tag{25}$$

$$\widetilde{\mathbf{P}} = \operatorname{diag}\left(\left[\widetilde{\mathbf{p}}_1^T\ \widetilde{\mathbf{p}}_2^T \cdots \widetilde{\mathbf{p}}_K^T\ \widetilde{p}_{K+1} \cdots \widetilde{p}_{K+NM}\right]\right) \tag{26}$$

with $\mathbf{A}_k = [\widetilde{\mathbf{a}}_{k1} \cdots \widetilde{\mathbf{a}}_{kM}]$, $\widetilde{\mathbf{p}}_k = [\widetilde{p}_{k1} \cdots \widetilde{p}_{kM}]^T$, $k = 1, \ldots, K$, and $\widetilde{\mathbf{a}}_{K+i}$ denoting the ith column of $\mathbf{I}_{NM}$, $i = 1, \ldots, NM$.

The first KM diagonal elements of $\widetilde{\mathbf{P}}$ (which are divided into K groups denoted $\{\widetilde{\mathbf{p}}_k\}_{k=1}^K$) represent the unknown powers of the grouped vector $\mathbf{x}$, and the last NM elements (which can be regarded as NM independent groups of size one) denote the unknown noise powers. Thus, the vector composed of the diagonal elements in $\widetilde{\mathbf{P}}$ denoted by $\widetilde{\mathbf{p}} \in \mathbb{C}^{KM+NM}$ is a group vector with $K + NM$ groups and the size of each group is equal to L_k, where

$$L_k = \begin{cases} M & k = 1, \cdots, K, \\ 1 & k = K+1, \cdots, K+NM. \end{cases} \tag{27}$$

Different from the single-snapshot SPICE algorithm [25], the following relaxed covariance fitting criterion is considered in the group SPICE approach to obtain a group sparse solution [33]:

$$\min_{\widetilde{\mathbf{p}} \geq 0} \widetilde{\mathbf{y}}^* \mathbf{R}_{\mathrm{g}}^{-1} \widetilde{\mathbf{y}} + \sum_{k=1}^{K+NM} \upsilon_k \|\widetilde{\mathbf{p}}_k\|_r \tag{28}$$

where $r \geq 1$, $s \geq 1$, $r^{-1} + s^{-1} = 1$, $\upsilon_k = \|\mathbf{w}_k\|_s$, and $\mathbf{w}_k = [\|\widetilde{\mathbf{a}}_{k1}\|_2^2 \cdots \|\widetilde{\mathbf{a}}_{kL_k}\|_2^2]$. It can be shown that under the assumption of heteroscedastic noise, the group SPICE problem in (28) is equivalent to the following optimization problem [33]:

$$\min_{\widetilde{\mathbf{x}}} \|\widetilde{\mathbf{y}} - \widetilde{\mathbf{B}}\widetilde{\mathbf{x}}\|_1 + \sqrt{NM^{1/s}} \sum_{k=1}^{K} \|\mathbf{x}_{k\cdot}\|_{\frac{2r}{r+1}} \tag{29}$$

which is a special case of the $l_{1,2r/r+1}$-PLAD below for $\lambda = \sqrt{NM^{1/s}}$

$$\min_{\mathbf{X}} \|\mathbf{Y} - \mathbf{B}\mathbf{X}\|_1 + \lambda \|\mathbf{X}\|_{1,\frac{2r}{r+1}}. \tag{30}$$

As $r \to \infty$, (29) becomes the $l_{1,2}$-PLAD approach in (11). Therefore, we can obtain $\mathbf{X}$ from the observed data matrix $\mathbf{Y}$ by approximately solving the $l_{1,2}$-PLAD problem (11) via the group SPICE algorithm with $r \gg 1$. The group SPICE algorithm is a good candidate for multiple-PRI-based RFI mitigation, but there still is a user parameter r to choose. The detailed steps of group SPICE are provided in [33]. In Section V, we will compare the group SPICE algorithm with the proposed version, which is presented in the following.

D. Modified Group SPICE

We now propose a modified group SPICE algorithm that, unlike group SPICE, is exactly equivalent to $l_{1,2}$-PLAD and does not require the selection of any user parameter. The modified group SPICE algorithm is obtained by assuming that each of the RFI sources has constant power within the CPI

$$\widetilde{p}_k = \widetilde{p}_{k1} = \widetilde{p}_{k2} = \cdots = \widetilde{p}_{kM} \tag{31}$$

for $k = 1, \ldots, K$. By substituting (31) into the relaxed covariance fitting criterion (28), we obtain the modified group SPICE criterion

$$\min_{\{\widetilde{p}_k \geq 0\}} \widetilde{\mathbf{y}}^* \mathbf{R}_{\mathrm{g}}^{-1} \widetilde{\mathbf{y}} + \sum_{k=1}^{K+NM} \|\widetilde{\mathbf{a}}_k\|_2^2 L_k \widetilde{p}_k \tag{32}$$

where $\|\widetilde{\mathbf{a}}_k\|_2^2 = \|\widetilde{\mathbf{a}}_{k1}\|_2^2 = \cdots = \|\widetilde{\mathbf{a}}_{kL_k}\|_2^2$ and we used the fact that $\upsilon_k {L_k}^{1/r} = \|\widetilde{\mathbf{a}}_k\|_2^2 {L_k}^{1/r+1/s} = \|\widetilde{\mathbf{a}}_k\|_2^2 \; L_k$. As it can be seen, the user parameter r has vanished from the criterion in (32).

Let the auxiliary variable $\boldsymbol{\beta} \in C^{KM+NM}$ be such that $\widetilde{\mathbf{A}}\boldsymbol{\beta} = \widetilde{\mathbf{y}}$. Then, consider the optimization problem

$$\min_{\{\widetilde{p}_k \geq 0\}, \boldsymbol{\beta}} \boldsymbol{\beta}^* \widetilde{\mathbf{P}}^{-1} \boldsymbol{\beta} + \sum_{k=1}^{K+NM} \|\widetilde{\mathbf{a}}_k\|_2^2 L_k \widetilde{p}_k \quad \text{s.t. } \widetilde{\mathbf{A}}\boldsymbol{\beta} = \widetilde{\mathbf{y}}. \tag{33}$$

The minimization of (33) with respect to $\boldsymbol{\beta}$ for fixed $\widetilde{\mathbf{P}}$ yields

$$\boldsymbol{\beta} = \widetilde{\mathbf{P}}\widetilde{\mathbf{A}}^* \mathbf{R}_{\mathrm{g}}^{-1} \widetilde{\mathbf{y}}. \tag{34}$$

Note that by inserting (34) into (33), we obtain (32), which shows that (32) and (33) have the same solution $\widetilde{\mathbf{P}}$.

Through using a cyclic minimization approach similar to that in [25], [26], and [33], the problem (33) can be conveniently solved by iteratively alternating between minimizing (33) with respect to $\boldsymbol{\beta}$ for fixed $\widetilde{\mathbf{P}}$ and minimizing (33) with respect to $\widetilde{\mathbf{P}}$ for given $\boldsymbol{\beta}$. The solution to the first step has been presented in (34). For completeness, we show below how to find a closed-form solution to the step of minimizing (32) with respect to $\widetilde{\mathbf{P}}$ for given $\boldsymbol{\beta}$. Let (33) be expressed as a separable optimization problem in the $K + NM$ groups as follows (for given $\boldsymbol{\beta}$):

$$\min_{\{\widetilde{p}_k\} \geq 0} \sum_{k=1}^{K+NM} \frac{\|\boldsymbol{\beta}_k\|_2^2}{\widetilde{p}_k} + \|\widetilde{\mathbf{a}}_k\|_2^2 L_k \widetilde{p}_k \tag{35}$$

where $\boldsymbol{\beta} = [\boldsymbol{\beta}_1^T \; \boldsymbol{\beta}_2^T \cdots \boldsymbol{\beta}_K^T \quad \beta_{K+1} \cdots \beta_{K+NM}]^T$, and $\boldsymbol{\beta}_k$ denotes the kth group of $\boldsymbol{\beta}$.

Applying the arithmetic–geometric mean inequality yields

$$\frac{\|\boldsymbol{\beta}_k\|_2^2}{\widetilde{p}_k} + \|\widetilde{\mathbf{a}}_k\|_2^2 L_k \widetilde{p}_k \geq 2\sqrt{\|\widetilde{\mathbf{a}}_k\|_2^2 L_k} \|\boldsymbol{\beta}_k\|_2. \tag{36}$$

Making use of (36), we obtain the solution to (35) as follows:

$$\widetilde{p}_k = \frac{\|\boldsymbol{\beta}_k\|_2}{\sqrt{\|\widetilde{\mathbf{a}}_k\|_2^2 L_k}} \tag{37}$$

and the corresponding minimum value of the objective is

$$\sum_{k=1}^{K+NM} 2\sqrt{\|\widetilde{\mathbf{a}}_k\|_2^2 L_k} \|\boldsymbol{\beta}_k\|_2. \tag{38}$$

Combining (34) and (37), the iterative steps of the hyperparameter-free modified group SPICE algorithm can be summarized as follows:

$$\widehat{\widetilde{p}}_k^{\,j+1} = \frac{\left\|\widehat{\widetilde{\mathbf{P}}}_k^{\,j} \mathbf{A}_k^* \widehat{\mathbf{R}}_{\mathrm{g}j}^{-1} \widetilde{\mathbf{y}}\right\|_2}{\sqrt{\|\widetilde{\mathbf{a}}_k\|_2^2 L_k}} \tag{39}$$

where $\widehat{\widetilde{\mathbf{P}}}_k^{\,j} = \mathrm{diag}(\widehat{\widetilde{\mathbf{p}}}_k^{\,j})$ for $k = 1, \ldots, K + NM$, and $\mathbf{A}_k = \widetilde{\mathbf{a}}_k$ for $k = K+1, \ldots, K+NM$.

Next, we will establish the relationship between the modified group SPICE criterion and the $l_{1,2}$-PLAD metric in (12).

Using (37), we can rewrite (33) as an objective function of $\boldsymbol{\beta}$ only [also see (38)]

$$\min_{\boldsymbol{\beta}} \sum_{k=1}^{K+NM} \sqrt{\|\widetilde{\mathbf{a}}_k\|_2^2 L_k}\|\boldsymbol{\beta}_k\|_2 \quad \text{s.t. } \widetilde{\mathbf{A}}\boldsymbol{\beta} = \widetilde{\mathbf{y}}. \tag{40}$$

Since the last NM groups of $\boldsymbol{\beta}$ are of size one, (40) can be rewritten as

$$\min_{\boldsymbol{\beta}} \sum_{k=1}^{K} \sqrt{\|\widetilde{\mathbf{a}}_k\|_2^2 L_k}\|\boldsymbol{\beta}_k\|_2 + \sum_{k=K+1}^{K+NM} \sqrt{\|\widetilde{\mathbf{a}}_k\|_2^2 L_k}|\boldsymbol{\beta}_k| \quad \text{s.t. } \widetilde{\mathbf{A}}\boldsymbol{\beta} = \widetilde{\mathbf{y}}. \tag{41}$$

In Appendix C, we show that the vector $\boldsymbol{\beta}$ that satisfies the constraint $\widetilde{\mathbf{A}}\boldsymbol{\beta} = \widetilde{\mathbf{y}}$ in (41) has the following general form:

$$\boldsymbol{\beta} = \begin{bmatrix} \widetilde{\mathbf{x}} \\ \widetilde{\mathbf{y}} - \widetilde{\mathbf{B}}\widetilde{\mathbf{x}} \end{bmatrix}. \tag{42}$$

Hence, the following optimization problem is equivalent to the one in (41):

$$\min_{\widetilde{\mathbf{x}}} \|\widetilde{\mathbf{y}} - \widetilde{\mathbf{B}}\widetilde{\mathbf{x}}\|_1 + \sqrt{MN}\sum_{k=1}^{K}\|\mathbf{x}_{k\cdot}\|_2. \tag{43}$$

Note that this equivalence can also be proved in a different way as shown in Appendix D. The first term in (43) is $\|\widetilde{\mathbf{e}}\|_1$, which is equivalent to the first term in (12), and the second term in (43) is $\sqrt{NM}\|\mathbf{X}\|_{1,2}$, which is equivalent to the second term in (12) with $\lambda = \sqrt{NM}$. Therefore, the modified group SPICE algorithm is equivalent to $l_{1,2}$-PLAD with $\lambda = \sqrt{MN}$.

To use the modified group SPICE algorithm for hyperparameter-free RFI mitigation in the multiple PRIs case, we initialize the algorithm with the power estimates obtained using the periodogram method (see [36]). We then iteratively update $\{\widehat{\widetilde{p}}_k\}_{k=1}^{K+NM}$ using (39) and estimate the RFI spectrum as $\{\widehat{\mathbf{x}}_{k\cdot} = (\widehat{\widetilde{\mathbf{P}}}_k\mathbf{A}_k^*\widehat{\mathbf{R}}_{\mathrm{g}}^{-1}\widetilde{\mathbf{y}})^T\}_{k=1}^{K}$ [see (34) and (42)]. Finally, the vectorized radar echo signal is obtained via $\widehat{\widetilde{\mathbf{s}}} = \widetilde{\mathbf{y}} - \widetilde{\mathbf{B}}\widehat{\widetilde{\mathbf{x}}}$.

As a final remark in this section, note that the RPCA algorithm [22] exploits a low-rank property of the RFI data matrix, whereas the group SPICE algorithms exploit its row-sparsity. While row-sparsity of a matrix implies low-rank, the converse is not necessarily true; therefore, row sparsity is a stricter and, thus, a more useful property for estimation purposes.

IV. Fast Implementations

In this section, we propose fast implementations of the proposed SPICE methods. We first present a fast implementation scheme for the single-snapshot SPICE using the CGLS approach [34], [35] and an FFT-based procedure to compute $\widehat{\mathbf{R}}^{-1}\mathbf{y}$. Then, we present a computationally efficient computation of $\widehat{\mathbf{R}}_{\mathrm{g}}^{-1}\widetilde{\mathbf{y}}$ for the group SPICE algorithms and explain how to compute the group SPICE estimates via the fast scheme proposed for the single-snapshot SPICE.

A. Fast Computation of $\widehat{\mathbf{R}}^{-1}\mathbf{y}$ in the Single-PRI Case

In the iterative framework of the single-snapshot SPICE, we need to recompute the covariance matrix $\widehat{\mathbf{R}}$ and its inverse at the current iteration from the power estimate $\widehat{\mathbf{P}}$ obtained in the previous iteration. The direct implementation of this step requires $O(N^2K)$ flops, which signifies a high computational complexity, especially because the number of grid points K is usually much larger than N. Inspired by the fast implementation idea in [34], we can save computations by exploiting the CGLS approach [35] to calculate $\widehat{\mathbf{R}}^{-1}\mathbf{y}$ without the formation of either $\widehat{\mathbf{R}}$ or $\widehat{\mathbf{R}}^{-1}$.

Define

$$\mathbf{D} = \begin{bmatrix} \boldsymbol{\Sigma}_1^{1/2}\mathbf{B}^* \\ \boldsymbol{\Sigma}_2^{1/2} \end{bmatrix} \quad \text{and } \mathbf{z} = \begin{bmatrix} \mathbf{0} \\ \boldsymbol{\Sigma}_2^{-1/2}\mathbf{y} \end{bmatrix} \quad \text{with } \boldsymbol{\Sigma}_1 = \mathrm{diag}([p_1 \cdots p_K]) \tag{44}$$

and

$$\boldsymbol{\Sigma}_2 = \mathrm{diag}([p_{K+1} \cdots p_{K+N}]). \tag{45}$$

We have

$$\widehat{\mathbf{R}}^{-1}\mathbf{y} = (\mathbf{B}\boldsymbol{\Sigma}_1\mathbf{B}^* + \boldsymbol{\Sigma}_2)^{-1}\mathbf{y} = (\mathbf{D}^*\mathbf{D})^{-1}\mathbf{D}^*\mathbf{z}. \tag{46}$$

It follows from (46) that $\mathbf{u} = \widehat{\mathbf{R}}^{-1}\mathbf{y}$ is also the solution of the following least squares problem [34]:

$$\min_{\mathbf{u}} \|\mathbf{D}\mathbf{u} - \mathbf{z}\|_2^2 \tag{47}$$

which can be efficiently solved by the CGLS algorithm [35].

Let $\mathbf{u}_0 = \mathbf{0}$, $\mathbf{s}_0 = \mathbf{z}$, $\mathbf{r}_0 = \mathbf{D}^*\mathbf{s}_0 = \mathbf{y}$ and $\mathbf{g}_0 = \mathbf{r}_0$. The lth iteration of the CGLS algorithm [35] can be expressed as follows.

1) $\mathbf{h}_l = \mathbf{D}^*\mathbf{D}\mathbf{g}_l = \mathbf{B}\boldsymbol{\Sigma_1}\mathbf{B}^*\mathbf{g}_l + \boldsymbol{\Sigma}_2\mathbf{g}_l$.
2) $\alpha_l = (\mathbf{r}_l^*\mathbf{r}_l/\mathbf{g}_l^*\mathbf{h}_l)$.
3) $\mathbf{u}_{l+1} = \mathbf{u}_l + \alpha_l\mathbf{g}_l$.
4) $\mathbf{r}_{l+1} = \mathbf{r}_l - \alpha_l\mathbf{h}_l$.
5) $\beta_l = (\mathbf{r}_{l+1}^*\mathbf{r}_{l+1}/\mathbf{r}_l^*\mathbf{r}_l)$.
6) $\mathbf{g}_{l+1} = \mathbf{r}_{l+1} + \beta_l\mathbf{g}_l$.

Since $\mathbf{B}$ is a Fourier transform matrix, $\mathbf{B}\mathbf{x}$ and $\mathbf{B}^*\mathbf{x}$ can be calculated by means of inverse FFT and FFT operations in $O(K\log_2 K)$ flops, respectively (here $\mathbf{x}$ is an arbitrary vector whose length is smaller than K). Moreover, we can compute $\boldsymbol{\Sigma}_1\mathbf{x}$ and $\boldsymbol{\Sigma}_2\mathbf{x}$ in $O(K)$ and $O(N)$ flops, respectively, because $\boldsymbol{\Sigma}_1$ and $\boldsymbol{\Sigma}_2$ are both diagonal matrices. Therefore, the first step of the CGLS iteration, which is the main computational step, has a reasonable computation complexity of $O(K\log_2 K)$. Assuming that $\widetilde{C}$ is the number of iterations needed by CGLS, which is related to the signal-to-interference ratio (SIR) of the observed RFI-contaminated signal rather than the size of the data [35], we can obtain $\widehat{\mathbf{R}}^{-1}\mathbf{y}$ using the CGLS and FFT in $O(\widetilde{C}K\log_2 K)$ flops. Compared to the $O(N^2K)$ flops required by the direct implementation of the single-snapshot SPICE algorithm, the proposed fast method has a significantly lower computational complexity. Note that the proposed fast implementation is also much faster than the direct minimization of the convex l_1-PLAD metric [31] using the interior point methods.

B. Fast Computation of $\widehat{\mathbf{R}}_{\mathrm{g}}^{-1}\widetilde{\mathbf{y}}$ in the Multiple PRIs Case

In the multiple PRIs case, the size of the covariance matrix $\widehat{\mathbf{R}}_{\mathrm{g}} \in \mathbb{C}^{NM\times NM}$ is quite large even for the moderate values of N and M. Therefore, the huge memory requirements alone can prevent the formation of the matrices $\widehat{\mathbf{R}}_{\mathrm{g}}$ and $\widetilde{\mathbf{B}}$. Moreover, even with sufficient memory, the direct calculation of $\widehat{\mathbf{R}}_{g}^{-1}\widetilde{\mathbf{y}}$ has a computational complexity of $O(N^2M^3K)$, resulting in a heavy computational burden. Fortunately, we can efficiently compute $\widehat{\mathbf{R}}_{g}^{-1}\widetilde{\mathbf{y}}$ by exploiting the special structure of $\widehat{\mathbf{R}}_{\mathrm{g}}$.

Using (23) and (25) in (24), the covariance matrix $\widehat{\mathbf{R}}_{\mathrm{g}}$ for the vectorized data $\widetilde{\mathbf{y}}$ can be rewritten as

$$\widehat{\mathbf{R}}_{\mathrm{g}} = \begin{bmatrix} \mathbf{A}\widehat{\widetilde{\mathbf{P}}}_1\mathbf{A}^* & \mathbf{0} & \cdots & \mathbf{0} \\ \mathbf{0} & \mathbf{A}\widehat{\widetilde{\mathbf{P}}}_2\mathbf{A}^* & \cdots & \mathbf{0} \\ \vdots & \vdots & \ddots & \vdots \\ \mathbf{0} & \mathbf{0} & \cdots & \mathbf{A}\widehat{\widetilde{\mathbf{P}}}_M\mathbf{A}^* \end{bmatrix} \tag{48}$$

where $\widehat{\widetilde{\mathbf{P}}}_m = \mathrm{diag}([\widehat{\widetilde{p}}_{1m}\cdots\widehat{\widetilde{p}}_{Km}\ \widehat{\widetilde{p}}_{K+(m-1)N+1}\cdots\widehat{\widetilde{p}}_{K+mN}])$ for $m = 1,\ldots,M$, and $\mathbf{A}$ is defined in (5). Apparently, $\widehat{\mathbf{R}}_{\mathrm{g}}$ is a block diagonal matrix whose mth diagonal block is equivalent to the covariance matrix of the data vector for the mth PRI. Let $\widehat{\mathbf{R}}_m = \mathbf{A}\widehat{\widetilde{\mathbf{P}}}_m\mathbf{A}^*$. Then,

$$\begin{aligned}\widehat{\mathbf{R}}_{\mathrm{g}}^{-1}\widetilde{\mathbf{y}} &= \begin{bmatrix} \widehat{\mathbf{R}}_1^{-1} & \mathbf{0} & \cdots & \mathbf{0} \\ \mathbf{0} & \widehat{\mathbf{R}}_2^{-1} & \cdots & \mathbf{0} \\ \vdots & \vdots & \ddots & \vdots \\ \mathbf{0} & \mathbf{0} & \cdots & \widehat{\mathbf{R}}_M^{-1} \end{bmatrix} \begin{bmatrix} \mathbf{y}_{\cdot 1} \\ \mathbf{y}_{\cdot 2} \\ \vdots \\ \mathbf{y}_{\cdot M} \end{bmatrix} \\ &= \begin{bmatrix} \widehat{\mathbf{R}}_1^{-1}\mathbf{y}_{\cdot 1} \\ \widehat{\mathbf{R}}_2^{-1}\mathbf{y}_{\cdot 2} \\ \vdots \\ \widehat{\mathbf{R}}_M^{-1}\mathbf{y}_{\cdot M} \end{bmatrix}. \end{aligned} \tag{49}$$

Therefore, we can obtain $\widehat{\mathbf{R}}_{\mathrm{g}}^{-1}\widetilde{\mathbf{y}}$ simply by computing $\{\widehat{\mathbf{R}}_m^{-1}\mathbf{y}_{\cdot m}\}_{m=1}^{M}$ via the fast implementation scheme proposed for the single-snapshot SPICE. The required computational cost is $O\left(\widetilde{C}MK\log_2 K\right)$, where $\widetilde{C}$ is the number of iterations needed by the CGLS algorithm (as in the Section IV-A).

V. Simulated Examples and Experimental Results

In this section, we evaluate the RFI mitigation performance of the SPICE algorithms and compare it with that of RPCA approach using both simulated and experimentally measured data. Specifically, our experiments are conducted using a measured RFI-free synthetic aperture radar (SAR) data set and two different RFI data sets: simulated RFI data and measured RFI data. The measured UWB SAR data set is collected by the ARL using the impulse-based low-frequency UWB BoomSAR system, with its transmitted signal frequency band from approximately 50 to 1150 MHz. The simulated RFI data set has the RFI sources generated as a sum of 10 sinusoidal signals, whereas the measured RFI data set is collected by the ARL radar receiver with the antenna pointing toward Washington, DC, USA (See [18], [19] for more details about the data collection using the ARL radar.) We first focus on the simulated RFI data set and then shift our attention to the measured RFI data set. The user parameter required by RPCA is set as recommended in [22] and its references. The size of the data set is $N = 2048$, $M = 1892$ and the number of grid points is $K = 20480$. The SAR images, denoted below using the symbol $\mathbf{Z}$, are obtained by applying the back-projection algorithm to the radar data both before and after RFI mitigation. Fig. 5 shows the original RFI-free SAR image. All the examples were run on a PC with 2.83-GHz CPU and 8.00-GB RAM.

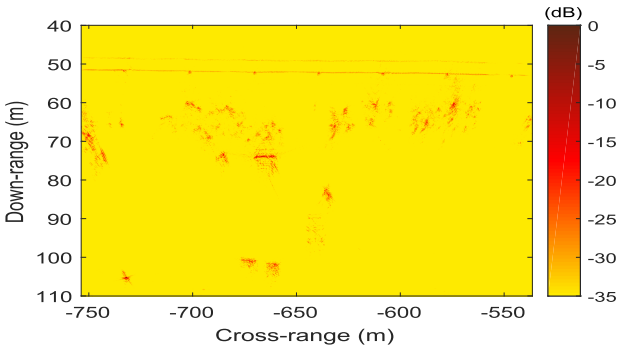

Fig. 5. Original RFI-free SAR image obtained by using the measured RFI-free UWB radar signal.

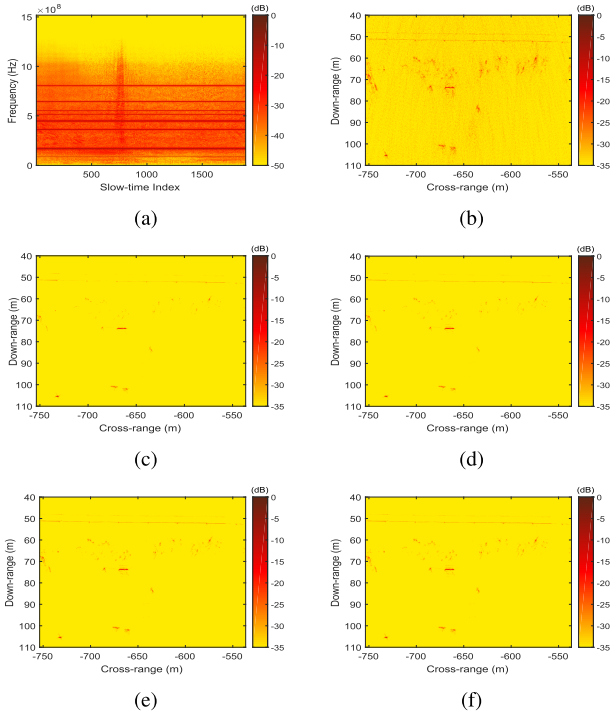

Fig. 6. RFI mitigation performance when the measured RFI-free UWB radar signal is contaminated by the simulated RFI. SIR $= -10$ dB. (a) Spectrum of RFI-contaminated data. (b) SAR image with RFI. (c) Recovered SAR image obtained by using the RPCA. (d) Recovered SAR image obtained by using the single-snapshot SPICE. (e) Recovered SAR image obtained by using the original group SPICE with $r = 25$. (f) Recovered SAR image obtained by using the modified group SPICE.

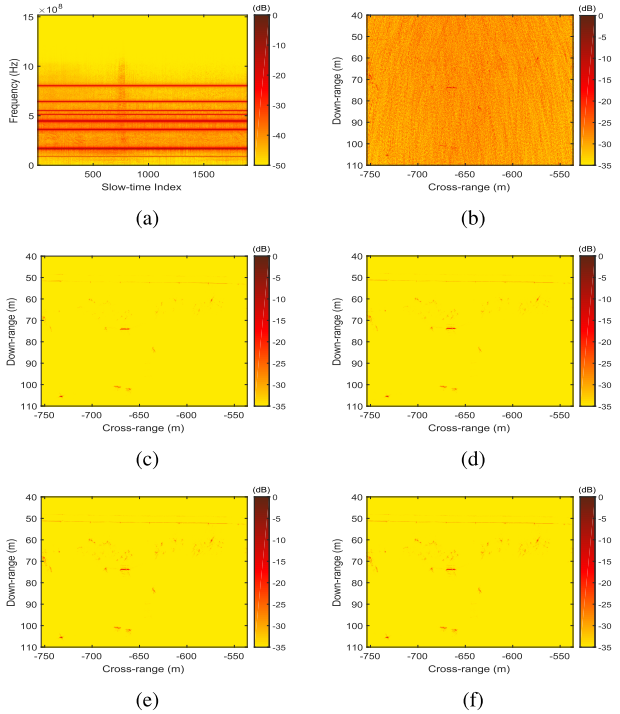

Fig. 7. RFI mitigation performance when the measured RFI-free UWB radar signal is contaminated by the simulated RFI. SIR $= -20$ dB. (a) Spectrum of RFI-contaminated data. (b) SAR image with RFI. (c) Recovered SAR image obtained by using the RPCA. (d) Recovered SAR image obtained by using the single-snapshot SPICE. (e) Recovered SAR image obtained by using the original group SPICE with $r = 25$. (f) Recovered SAR image obtained by using the modified group SPICE.

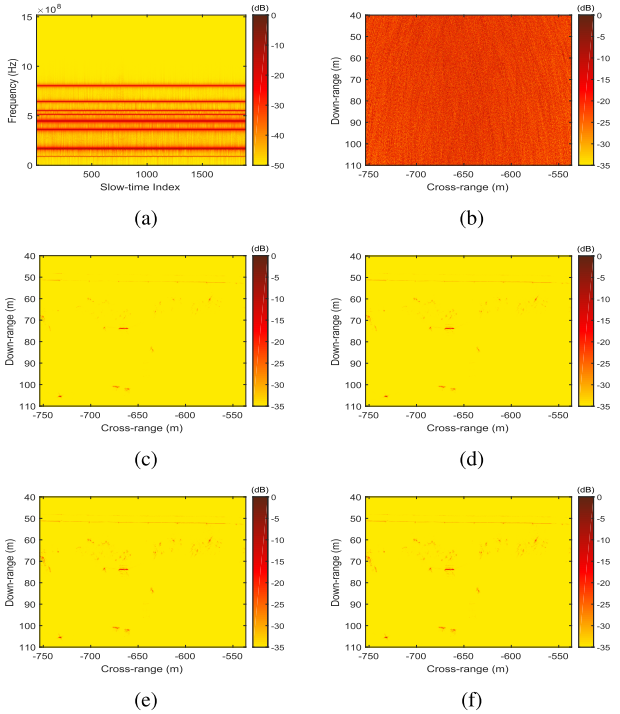

Fig. 8. RFI mitigation performance when the measured RFI-free UWB radar signal is contaminated by the simulated RFI. SIR $= -30$ dB. (a) Spectrum of RFI-contaminated data. (b) SAR image with RFI. (c) Recovered SAR image obtained by using the RPCA. (d) Recovered SAR image obtained by using the single-snapshot SPICE. (e) Recovered SAR image obtained by using the original group SPICE with $r = 25$. (f) Recovered SAR image obtained by using the modified group SPICE.

A. Evaluation Metric

To evaluate the intensity of the interference signal before RFI mitigation, the SIR is defined as

$$\mathrm{SIR} = 20\log_{10}\frac{\|\mathbf{S}\|_F}{\|\mathbf{BX}\|_F}. \tag{50}$$

The received RFI-contaminated radar data are obtained by adjusting the RFI data power based on the desired SIR and then adding it to the RFI-free UWB radar signal. Note that both the measured RFI-free UWB radar signal and the measured RFI data set inevitably contain noise caused by the experimental ARL radar system. Hence, as we lower the SIR value, we are lowering the SNR value of the received radar data as well. Similar to [22]–[24], we utilize the SNR of the recovered SAR image to benchmark the RFI mitigation performance

$$\mathrm{SNR_Z} = 20\log_{10}\frac{\|\widetilde{\mathbf{Z}}_0\|_F}{\|\widetilde{\mathbf{Z}}_0 - \widehat{\widetilde{\mathbf{Z}}}\|_F} \tag{51}$$

where $\widetilde{\mathbf{Z}}_0$ and $\widehat{\widetilde{\mathbf{Z}}}$ are the original RFI-free SAR image and recovered SAR image, which are normalized to have the same $\|\cdot\|_F = 1$, respectively.

B. Results for Simulated RFI

In this section, the measured RFI-free UWB radar signal is contaminated by the simulated RFI data to obtain the RFI-contaminated radar data set. The parameter r needed by the original group SPICE is set to 25. The SIR values in the three cases of this experiment are -10, -20, and -30 dB, respectively, and Figs. 6–8 show the corresponding results. Figs. 6–8(b) show the RFI-contaminated SAR images. It is obvious that the presence of strong RFI sources can bury the targets of interest and severely degrade the quality of the SAR images. Fig. 6(c)–(f), Fig. 7(c)–(f), and Fig. 8(c)–(f), respectively, show the recovered SAR images after RFI mitigation using the RPCA, the single-snapshot SPICE, the original group SPICE with $r = 25$, and the modified group SPICE. Note that the single-snapshot SPICE is applied to each column of $\mathbf{Y}$.

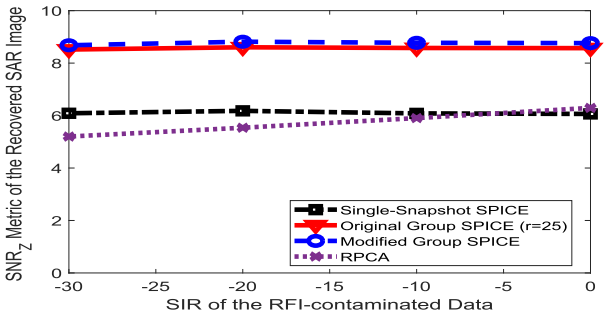

Fig. 9. RFI mitigation performance of the single-snapshot SPICE, the original group SPICE with $r = 25$, the modified group SPICE, and the RPCA, for various SIR values, when the measured RFI-free UWB radar signal is contaminated by the simulated RFI.

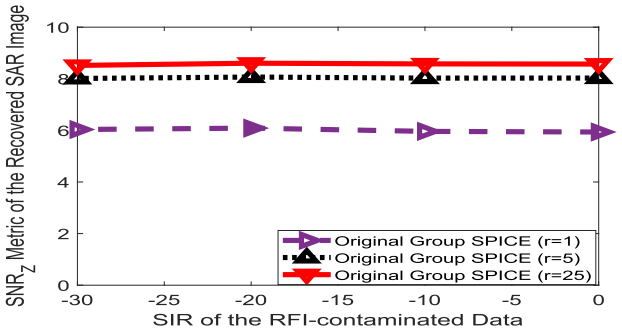

Fig. 10. RFI mitigation performance of the original group SPICE for various SIR values and r values when the measured RFI-free UWB radar signal is contaminated by the simulated RFI.

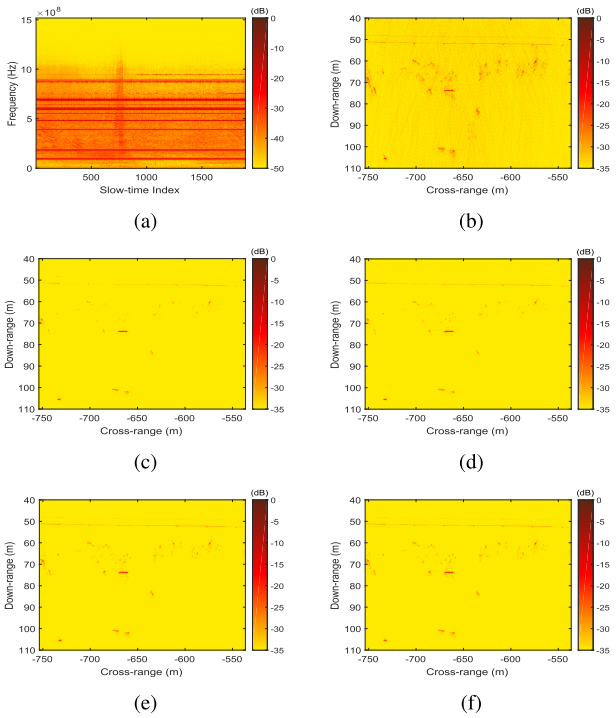

Fig. 11. RFI mitigation performance when the measured RFI-free UWB radar signal is contaminated by the measured RFI. SIR $= -10$ dB. (a) Spectrum of RFI-contaminated data. (b) SAR image with RFI. (c) Recovered SAR image obtained by using the RPCA. (d) Recovered SAR image obtained by using the single-snapshot SPICE. (e) Recovered SAR image obtained by using the riginal group SPICE with $r = 25$. (f) Recovered SAR image obtained by using the modified group SPICE.

Visually, the recovered SAR images obtained by using the RPCA algorithm are much sparser than the original RFI-free SAR image, and some weak targets are lost. All SPICE algorithms significantly outperform the RPCA approach. In addition, due to utilizing the row-sparsity within the CPI, the group SPICE algorithms outperform the single-snapshot SPICE, with many weak targets still being visually detectable after RFI mitigation using the group SPICE algorithms. The recovered SAR images obtained by using the modified group SPICE are visually similar to those obtained by using the original group SPICE with $r = 25$, as might have been expected.

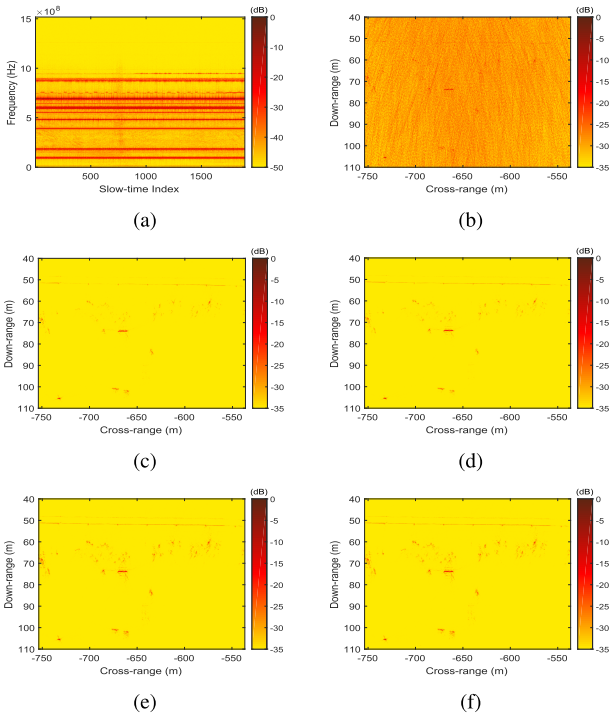

Fig. 12. RFI mitigation performance when the measured RFI-free UWB radar signal is contaminated by the measured RFI. SIR $= -20$ dB. (a) Spectrum of RFI-contaminated data. (b) SAR image with RFI. (c) Recovered SAR image obtained by using the RPCA. (d) Recovered SAR image obtained by using the single-snapshot SPICE. (e) Recovered SAR image obtained by using the original group SPICE with $r = 25$. (f) Recovered SAR image obtained by using the modified group SPICE.

Figs. 9 and 10 compare the RFI mitigation performance using the SNR_Z metric in (48) for the aforementioned four methods over a large range of SIR. The parameter r needed by the original group SPICE is set to 1, 5, and 25. The SNR curves in Figs. 9 and 10 show that in the case of simulated RFI, the recovered SAR images of all four algorithms appear to be affected insignificantly by the SIR values, which indicates excellent RFI mitigation performance. In addition, in terms of the SNR_Z values of the recovered SAR images, the original group SPICE appears to perform worse as r decreased. The modified group SPICE algorithm and the original group SPICE algorithm with a large r (for example $r = 25$) outperform the single-snapshot SPICE and the RPCA by about 3 dB in terms of the SNR_Z values. The single-snapshot SPICE algorithm outperforms the RPCA for low SIR values.

C. Results for Measured RFI

Figs. 11–13 present the RFI mitigation results using the measured RFI data set and the measured RFI-free UWB radar signal. The parameter r needed by the original group SPICE is set to 25 as before. The SIR values are also -10, -20, and -30 dB, respectively. As shown in Figs. 11–13(a), the spectra of the measured RFI-contaminated data are relatively similar to the spectra of their simulated counterparts in Figs. 6–8(a). For an SIR value of -10 or -20 dB, all details in the original SAR image are discernable in the images obtained using the group SPICE algorithms, while some weak targets

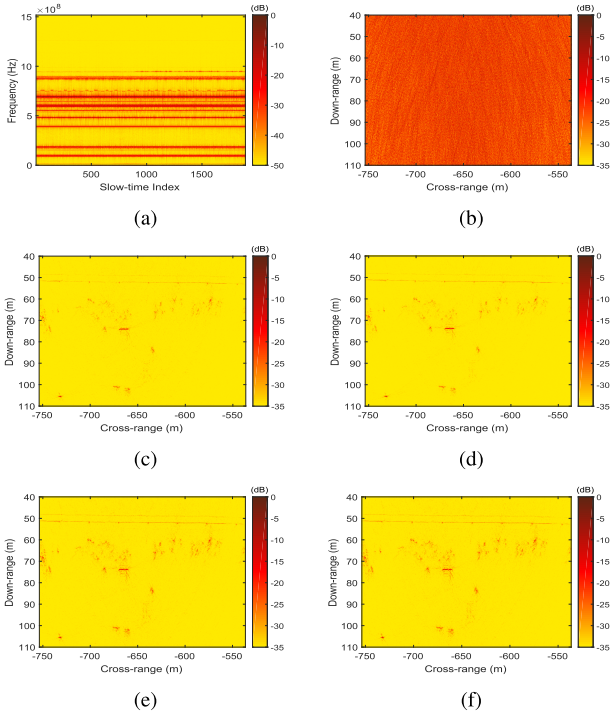

Fig. 13. RFI mitigation performance when the measured RFI-free UWB radar signal is contaminated by the measured RFI. SIR $= -30$ dB. (a) Spectrum of RFI-contaminated data. (b) SAR image with RFI. (c) Recovered SAR image obtained by using the RPCA. (d) Recovered SAR image obtained by using the single-snapshot SPICE. (e) Recovered SAR image obtained by using the original group SPICE with $r = 25$. (f) Recovered SAR image obtained by using the modified group SPICE.

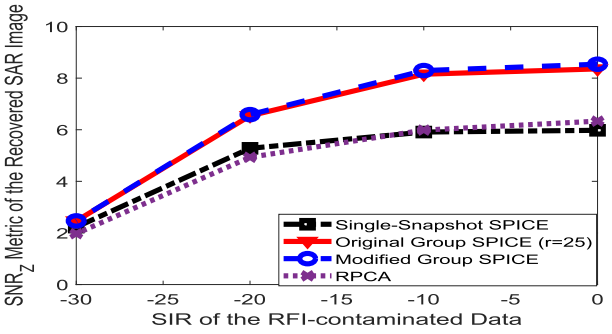

Fig. 14. RFI mitigation performance of the single-snapshot SPICE, the original group SPICE with $r = 25$, the modified group SPICE and the RPCA, for various SIR values, when the measured RFI-free UWB radar signal is contaminated by the measured RFI.

are missing in the recovered SAR images obtained using the single-snapshot SPICE and RPCA. For the more challenging case of SIR $= -30$ dB, most of the features are retained in the resulting SAR images obtained by the group SPICE algorithms, although obviously their noise levels are now higher. As already mentioned, this is due to the fact that the measured RFI data set contains noise, and lowering the SIR value increases the noise power. In addition, compared with the image obtained by the RPCA algorithm, in which some weak targets are missing and the high noise level is fairly high, the SAR image obtained using the single-snapshot SPICE, though with some details missing, has a lower noise level.

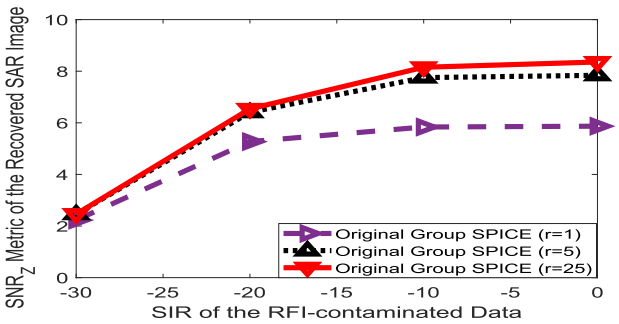

Fig. 15. RFI mitigation performance of the original group SPICE for various SIR values and r values when the measured RFI-free UWB radar signal is contaminated by the measured RFI.

Figs. 14 and 15 compare the SNR_Z metrics in (51) associated with the recovered SAR images, for various SIR values. The parameter r needed by the original group SPICE is set to 1, 5, and 25. The SNR_Z values of the recovered SAR images are affected by the SIR values due to the presence of noise in the measured RFI data set. The results obtained by the original group SPICE are affected by the choice of r. The original group SPICE provides a worse RFI mitigation performance as r decreases. The modified group SPICE algorithm and the original group SPICE algorithm with a large r (for example, $r = 25$) outperform their single-snapshot SPICE and RPCA counterparts as SIR varies from -30 to 0 dB. The single-snapshot SPICE algorithm performs slightly better than RPCA for low SNR values.

D. Computational Time

For the data vector from a single PRI, i.e., one column of the RFI-contaminated data matrix, with an SIR $= -30$ dB, the computational times required by the fast and direct implementations of the single-snapshot SPICE are about 6 and 2719 s, respectively. Hence, the proposed fast implementation scheme results in a considerable reduction in the computational complexity of the single-snapshot SPICE. For the RFI-contaminated data matrix collected over multiple PRIs with the size $N = 2048$ and $M = 1892$, the covariance matrix has very large dimensions and the resulting 3874816×3874816 array exceeds the maximum size limit of MATLAB, making the direct implementation impossible. In contrast with this, using the fast computation proposed for group SPICE, the creation of the covariance matrix and other large matrices is avoided and the required computational time of group SPICE is only about M times larger than when applying the single-snapshot SPICE to a single-PRI data vector.

VI. Conclusion

In this paper, we have presented a novel framework, based on proper data models, for hyperparameter-free RFI mitigation in either single PRI or multiple PRIs (within a CPI) cases. In the single PRI case, we have used the single-snapshot SPICE algorithm, which is a special case of the l_1-PLAD approach, for RFI mitigation. In the multiple PRIs case,

we have introduced a modified group SPICE algorithm for effective RFI mitigation, which was proven to be a special case of the $l_{1,2}$-PLAD approach. These methods simultaneously enforce the sparsity properties of UWB radar echoes and RFI spectrum. In addition, the proposed methods do not require the tuning of any user parameter nor the collection of any prior information on the RFI. We have also presented fast implementations of the SPICE algorithms. Experiments based on both simulated and measured data have been used to demonstrate the effectiveness of our methods. The proposed modified group SPICE algorithm has been shown to outperform both the single-snapshot SPICE algorithm and the RPCA approach for a wide range of SIR values.

Appendix A
Null Space of $\mathbf{A}$

From Equation (5), we have that $\mathbf{A}$ is of dimension $N\times(N+K)$ since $\mathbf{B}$ is of dimension $N\times K$. Clearly, $\text{rank}(\mathbf{A}) = N$. Therefore, the dimension of the null space of $\mathbf{A}$ is K. The $(N+K)\times K$ matrix

$$\begin{bmatrix}\mathbf{I}_K\\ -\mathbf{B}\end{bmatrix} \tag{52}$$

is in the null space of $\mathbf{A}$ and its rank is K. Thus, the columns of the matrix in (52) form a basis for the null space of $\mathbf{A}$.

Appendix B
Proof of Equation (17)

Consider the $N\times M$ matrix $\mathbf{Y}$, $N\times K$ matrix $\mathbf{B}$, and $K\times M$ matrix $\mathbf{X}$. We have $K > N$ (usually $K \gg N$), but M may or may not be larger than N. By using (13) in the linear constraint in (16), we obtain

$$\mathbf{AC} = \frac{\mathbf{YY}^*}{M} \tag{53}$$

where $\mathbf{C}$ is a $(K+N)\times N$ matrix and $\mathbf{A}$ is defined in (5). A particular solution to (53) is

$$\mathbf{C} = \begin{bmatrix}\mathbf{0}\\ \frac{\mathbf{YY}^*}{M}\end{bmatrix} \tag{54}$$

and therefore a general solution to (53) is (using the result in Appendix A on the null space of $\mathbf{A}$)

$$\mathbf{C} = \begin{bmatrix}\mathbf{0}\\ \frac{\mathbf{YY}^*}{M}\end{bmatrix} + \begin{bmatrix}\mathbf{I}_K\\ -\mathbf{B}\end{bmatrix}\mathbf{Z} \tag{55}$$

where $\mathbf{Z}$ is an arbitrarily $K\times N$ matrix. Assume that $M \geq N$ and that the determinant of $\widehat{\mathbf{R}}$ is nonzero. Let the $K\times M$ matrix $\mathbf{X}$ be

$$\mathbf{X} = \mathbf{Z}\left(\frac{\mathbf{YY}^*}{M}\right)^{-1}\mathbf{Y}. \tag{56}$$

Clearly $\mathbf{X}(\mathbf{Y}^*/M) = \mathbf{Z}$, and therefore, we can overparameterize (55) via $\mathbf{X}$

$$\mathbf{C} = \begin{bmatrix}\mathbf{0}\\ \frac{\mathbf{YY}^*}{M}\end{bmatrix} + \begin{bmatrix}\mathbf{I}_K\\ -\mathbf{B}\end{bmatrix}\mathbf{X}\frac{\mathbf{Y}^*}{M} = \begin{bmatrix}\mathbf{X}\\ \mathbf{Y}-\mathbf{BX}\end{bmatrix}\frac{\mathbf{Y}^*}{M} \tag{57}$$

which proves (17).

Appendix C
Proof of Equation (42)

Consider the constraint in (41)

$$\widetilde{\mathbf{A}}\boldsymbol{\beta} = \widetilde{\mathbf{y}}. \tag{58}$$

We want to find the solution $\boldsymbol{\beta}$ to (58).

We have

$$\widetilde{\mathbf{A}} = [\widetilde{\mathbf{B}}\ \mathbf{I}_{NM}] \tag{59}$$

where $\widetilde{\mathbf{B}}$ is an $(NM)\times(KM)$ matrix and hence $\widetilde{\mathbf{A}}$ is an $(NM)\times(NM+KM)$ matrix. Clearly, $\text{rank}\left(\widetilde{\mathbf{A}}\right) = NM$. Then, using the discussion in Appendix A, we have that the columns of

$$\begin{bmatrix}\mathbf{I}_{KM}\\ -\widetilde{\mathbf{B}}\end{bmatrix} \tag{60}$$

form a basis for the null space of $\widetilde{\mathbf{A}}$. This observation implies that the general solution of (58) can be written as

$$\boldsymbol{\beta} = \begin{bmatrix}\mathbf{0}\\ \widetilde{\mathbf{y}}\end{bmatrix} + \begin{bmatrix}\mathbf{I}_{KM}\\ -\widetilde{\mathbf{B}}\end{bmatrix}\widetilde{\mathbf{x}} = \begin{bmatrix}\widetilde{\mathbf{x}}\\ \widetilde{\mathbf{y}}-\widetilde{\mathbf{B}}\widetilde{\mathbf{x}}\end{bmatrix} \tag{61}$$

where $\widetilde{\mathbf{x}}$ is an arbitrary KM-dimensional vector. This concludes the proof of (42).

Appendix D
Another Proof of Equation (43)

To prove the connection between the modified group SPICE and $l_{1,2}$-PLAD from another perspective, we first recall the following lemma (see [27], [30]).

Lemma 1: Let

$$\boldsymbol{\Pi}_1 = \text{diag}\left(\left[\widetilde{\mathbf{p}}_1^T\ \widetilde{\mathbf{p}}_2^T\cdots\widetilde{\mathbf{p}}_K^T\right]\right) \tag{62}$$

and

$$\boldsymbol{\Pi}_2 = \text{diag}\left(\left[\widetilde{p}_{K+1}^T\ \widetilde{p}_{K+2}^T\cdots\widetilde{p}_{K+NM}^T\right]\right). \tag{63}$$

Then,

$$\widetilde{\mathbf{y}}^*\mathbf{R}_g^{-1}\widetilde{\mathbf{y}} = \min_{\widetilde{\mathbf{x}}}(\widetilde{\mathbf{y}}-\widetilde{\mathbf{B}}\widetilde{\mathbf{x}})^*\boldsymbol{\Pi}_2^{-1}(\widetilde{\mathbf{y}}-\widetilde{\mathbf{B}}\widetilde{\mathbf{x}}) + \sum_{k=1}^{K}\|\mathbf{x}_{k\cdot}\|_2^2/\widetilde{p}_k \tag{64}$$

and the minimum value occurs at

$$\widehat{\widetilde{\mathbf{x}}} = \boldsymbol{\Pi}_1\widetilde{\mathbf{B}}^*\mathbf{R}_g^{-1}\widetilde{\mathbf{y}}. \tag{65}$$

Making use of this lemma, we can rewrite (32) as

$$\min_{\{\widetilde{p}_k\geq 0\},\widetilde{\mathbf{x}}}\sum_{l=1}^{NM}|\ \widetilde{y}_l - \widetilde{\mathbf{B}}_{l\cdot}\widetilde{\mathbf{x}}\ |^2\ /\widetilde{p}_{K+l} + \sum_{k=1}^{K}\|\mathbf{x}_{k\cdot}\|_2^2/\widetilde{p}_k + \sum_{k=1}^{K+NM}\|\widetilde{\mathbf{a}}_k\|_2^2 L_k\widetilde{p}_k \tag{66}$$

where $\widetilde{y}_l$ denotes the lth element of $\widetilde{\mathbf{y}}$, and $\widetilde{\mathbf{B}}_{l\cdot}$ is the lth row of $\widetilde{\mathbf{B}}$. The minimization of (66) with respect to $\{p_k\}_{k=1}^{K+NM}$ yields

$$\widetilde{p}_k = \frac{\|\mathbf{x}_{k\cdot}\|_2}{\sqrt{\|\widetilde{\mathbf{a}}_k\|_2^2 L_k}}\quad \text{for } k = 1,\ldots,K \tag{67}$$

and

$$\widetilde{p}_{K+l} = \frac{|\ \widetilde{y}_l - \widetilde{\mathbf{B}}_l.\widetilde{\mathbf{x}}\ |}{\sqrt{\|\widetilde{\mathbf{a}}_{K+l}\|_2^2 L_{K+l}}} \quad \text{for } l = 1, \ldots, NM. \tag{68}$$

Inserting (67), (68), (27), and the value of $\{\|\widetilde{\mathbf{a}}_k\|_2\}_{k=1}^{K+NM}$ into (66), we conclude that the modified group SPICE metric is equivalent to (43), which is shown to be the vector form of $l_{1,2}$-PLAD. Therefore, the modified group SPICE is equivalent to the $l_{1,2}$-PLAD optimization metric with a particular choice of the hyperparameter.

REFERENCES

[1] J. D. Taylor, *Ultra-Wideband Radar Technology*. Boca Raton, FL, USA: CRC Press, 2000.

[2] A. Moreira, P. Prats-Iraola, M. Younis, G. Krieger, I. Hajnsek, and K. P. Papathanassiou, "A tutorial on synthetic aperture radar," *IEEE Geosci. Remote Sens. Mag.*, vol. 1, no. 1, pp. 6–43, Mar. 2013.

[3] L. H. Nguyen, K. A. Kappra, D. C. Wong, R. Kapoor, and J. Sichina, "Mine field detection algorithm utilizing data from an ultrawideband wide-area surveillance radar," *Proc. SPIE*, vol. 3392, pp. 627–643, Sep. 1998.

[4] L. H. Nguyen, M. Ressler, and J. Sichina, "Sensing through the wall imaging using the Army Research Lab Ultra-Wideband Synchronous Impulse Reconstruction (UWB SIRE) radar," *Proc. SPIE*, vol. 6947, p. 69470B, Apr. 2008.

[5] M. A. Ressler, "The army research laboratory ultra wideband Boom-SAR," in *Proc. IEEE Geosci. Remote Sens. Symp. (IGARSS)*, vol. 3, May 1996, pp. 1886–1888.

[6] T. Koutsoudis and L. A. Lovas, "RF interference suppression in ultrawideband radar receivers," *Proc. SPIE*, vol. 2487, pp. 107–118, Jun. 1995.

[7] D. O. Carhoun, "Adaptive nulling and spatial spectral estimation using an iterated principal components decomposition," in *Proc. Int. Conf. Acoust., Speech, Signal Process.*, vol. 5, Apr. 1991, pp. 3309–3312.

[8] H. Subbaram and K. Abend, "Interference suppression via orthogonal projections: A performance analysis," *IEEE Trans. Antennas Propag.*, vol. 41, no. 9, pp. 1187–1194, Sep. 1993.

[9] M. Ghadaksaz, "Novel active RF tracking notch filters for interference suppression in HF, VHF, and UHF frequency hopping receivers," in *Proc. Conf. Rec. MILCOM*, vol. 3, Nov. 1991, pp. 956–960.

[10] V. T. Vu, T. K. Sjögren, M. I. Pettersson, and L. Håkansson, "An approach to suppress RFI in ultrawideband low frequency SAR," in *Proc. IEEE Radar Conf.*, May 2010, pp. 1381–1385.

[11] X. Luo, L. M. H. Ulander, J. Askne, G. Smith, and P. O. Frolind, "RFI suppression in ultra-wideband SAR systems using LMS filters in frequency domain," *Electron. Lett.*, vol. 37, no. 4, pp. 241–243, Feb. 2001.

[12] T. Miller, L. Potter, and J. McCorkle, "RFI suppression for ultra wideband radar," *IEEE Trans. Aerosp. Electron. Syst.*, vol. 33, no. 4, pp. 1142–1156, Oct. 1997.

[13] X. Y. Wang, W. D. Yu, X. Y. Qi, and Y. Liu, "RFI suppression in SAR based on approximated spectral decomposition algorithm," *Electron. Lett.*, vol. 48, no. 10, pp. 594–596, May 2012.

[14] F. Zhou, R. Wu, M. Xing, and Z. Bao, "Eigensubspace-based filtering with application in narrow-band interference suppression for SAR," *IEEE Geosci. Remote Sens. Lett.*, vol. 4, no. 1, pp. 75–79, Jan. 2007.

[15] F. Zhou, M. Tao, X. Bai, and J. Liu, "Narrow-band interference suppression for SAR based on independent component analysis," *IEEE Trans. Geosci. Remote Sens.*, vol. 51, no. 10, pp. 4952–4960, Oct. 2013.

[16] F. Zhou and M. Tao, "Research on methods for narrow-band interference suppression in synthetic aperture radar data," *IEEE J. Sel. Topics Appl. Earth Observ. Remote Sens.*, vol. 8, no. 7, pp. 3476–3485, Jul. 2015.

[17] L. H. Nguyen and T. D. Tran, "Robust and adaptive extraction of RFI signals from ultra-wideband radar data," in *Proc. IEEE Geosci. Remote Sens. Symp. (IGARSS)*, Jun. 2012, pp. 7137–7140.

[18] L. H. Nguyen and T. D. Tran, "Efficient and robust RFI extraction via sparse recovery," *IEEE J. Sel. Topics Appl. Earth Observ. Remote Sens.*, vol. 9, no. 6, pp. 2104–2117, Jun. 2016.

[19] L. H. Nguyen, T. Tran, and T. Do, "Sparse models and sparse recovery for ultra-wideband SAR applications," *IEEE Trans. Aerosp. Electron. Syst.*, vol. 50, no. 2, pp. 940–958, Apr. 2014.

[20] L. H. Nguyen, M. D. Dao, and T. D. Tran, "Radio-frequency interference separation and suppression from ultrawideband radar data via low-rank modeling," in *Proc. IEEE Int. Conf. Image Process. (ICIP)*, Oct. 2014, pp. 116–120.

[21] L. H. Nguyen, M. D. Dao, and T. D. Tran, "Joint sparse and low-rank model for radio-frequency interference suppression in ultra-wideband radar applications," in *Proc. 48th Asilomar Conf. Signals, Syst. Comput.*, Nov. 2014, pp. 864–868.

[22] L. H. Nguyen and T. D. Tran, "RFI-radar signal separation via simultaneous low-rank and sparse recovery," in *Proc. IEEE Radar Conf. (RadarConf)*, May 2016, pp. 1–5.

[23] L. H. Nguyen and T. D. Tran, "A comprehensive performance comparison of RFI mitigation techniques for UWB radar signals," in *Proc. IEEE Int. Conf. Acoust., Speech Signal Process. (ICASSP)*, Mar. 2017, pp. 3086–3090.

[24] L. H. Nguyen and T. D. Tran, "Interference separation for UWB radar signals from entropy-driven robust PCA," in *Proc. IEEE Radar Conf. (RadarConf)*, May 2017, pp. 389–393.

[25] P. Stoica, P. Babu, and J. Li, "New method of sparse parameter estimation in separable models and its use for spectral analysis of irregularly sampled data," *IEEE Trans. Signal Process.*, vol. 59, no. 1, pp. 35–47, Jan. 2011.

[26] P. Stoica, P. Babu, and J. Li, "SPICE: A sparse covariance-based estimation method for array processing," *IEEE Trans. Signal Process.*, vol. 59, no. 2, pp. 629–638, Feb. 2011.

[27] P. Stoica, D. Zachariah, and J. Li, "Weighted SPICE: A unifying approach for hyperparameter-free sparse estimation," *Digit. Signal Process.*, vol. 33, pp. 1–12, Oct. 2014.

[28] C. R. Rojas, D. Katselis, and H. Hjalmarsson, "A note on the SPICE method," *IEEE Trans. Signal Process.*, vol. 61, no. 18, pp. 4545–4551, Sep. 2013.

[29] P. Babu and P. Stoica, "Connection between SPICE and square-root LASSO for sparse parameter estimation," *Signal Process.*, vol. 95, pp. 10–14, Feb. 2014.

[30] J. Swärd, S. I. Adalbjörnsson, and A. Jakobsson, "Generalized sparse covariance-based estimation," *Signal Process.*, vol. 143, pp. 311–319, Feb. 2018.

[31] L. Wang, "The L_1 penalized LAD estimator for high dimensional linear regression," *J. Multivariate Anal.*, vol. 120, pp. 135–151, Sep. 2013.

[32] A. Belloni, V. Chernozhukov, and L. Wang, "Square-root lasso: Pivotal recovery of sparse signals via conic programming," *Biometrika*, vol. 98, no. 4, pp. 791–806, 2011.

[33] T. Kronvall, S. I. Adalbjörnsson, S. Nadig, and A. Jakobsson, "Group-sparse regression using the covariance fitting criterion," *Signal Process.*, vol. 139, pp. 116–130, Oct. 2017.

[34] X. Tan, W. Roberts, J. Li, and P. Stoica, "Sparse learning via iterative minimization with application to MIMO radar imaging," *IEEE Trans. Signal Process.*, vol. 59, no. 3, pp. 1088–1101, Mar. 2011.

[35] R. C. Aster, B. Borchers, and C. H. Thurber, *Parameter Estimation and Inverse Problems*, vol. 90. New York, NY, USA: Academic, 2011.

[36] P. Stoica and R. L. Moses, *Spectral Anal. Signals*. Upper Saddle River, NJ, USA: Prentice-Hall, 2005.

Jiaying Ren received the B.S. degree in applied physics from the University of Science and Technology of China, Hefei, China, in 2016.

She is currently with the Department of Electrical and Computer Engineering, University of Florida, Gainesville, FL, USA. Her research interests include spectral estimation, statistical signal processing, and their applications.

Tianyi Zhang received the B.S.E.E. degree in electrical engineering from the University of Science and Technology of China, Hefei, China, in 2017. He is currently pursuing the Ph.D. degree with the Department of Electrical and Computer Engineering, University of Florida, Gainesville, FL, USA.

His research interests include spectral estimation, statistical signal processing, and their applications.

Jian Li (F'05) received the M.Sc. and Ph.D. degrees in electrical engineering from The Ohio State University, Columbus, OH, USA, in 1987 and 1991, respectively.

She is currently a Professor with the Department of Electrical and Computer Engineering, University of Florida, Gainesville, FL, USA. She has co-authored several papers in the IEEE TRANSACTIONS ON AEROSPACE AND ELECTRONIC SYSTEMS and the IEEE TRANSACTIONS ON SIGNAL PROCESSING. She has authored or co-authored several books including *Robust Adaptive Beamforming* (Wiley, 2005), *Spectral Analysis: the Missing Data Case* (Morgan and Claypool, 2005), *Multiple-Input Multiple-Output Radar Signal Processing* (Wiley, 2009), and *Waveform Design for Active Sensing Systems—A Computational Approach* (Cambridge University Press, 2011). Her research interests include spectral estimation, statistical and array signal processing, and their applications to radar, sonar, and biomedical engineering.

Dr. Li is a Fellow of IET and European Academy of Sciences, Brussels. She was an Executive Committee Member of the 2002 International Conference on Acoustics, Speech, and Signal Processing, Orlando, Florida, a member of the Editorial Board of Signal Processing, a publication of the European Association for Signal Processing, from 2005 to 2007, and a member of the Editorial Board of the IEEE *Signal Processing Magazine* from 2010 to 2012. She serves as a member for the Sensor Array and Multichannel Technical Committee of the IEEE Signal Processing Society. She was a recipient of the 1994 National Science Foundation Young Investigator Award, the 1996 Office of Naval Research Young Investigator Award, the M. Barry Carlton Award in 2005, and the Best Paper Award from the IEEE Signal Processing Society. She served as an Associate Editor for the IEEE TRANSACTIONS ON SIGNAL PROCESSING from 1999 to 2005 and *IEEE Signal Processing Magazine* from 2003 to 2005.

Lam H. Nguyen received the B.S.E.E. degree from the Virginia Polytechnic Institute, Blacksburg, VA, USA, in 1984, the M.S.E.E. degree from George Washington University, Washington, DC, USA, in 1991, and the M.S.C.S. degree from Johns Hopkins University, Baltimore, MD, USA, in 1995.

In 1984, he was with General Electric Company, Portsmouth, VA, USA. Since 1986, he has been with the Harry Diamond Laboratory, Adelphi, MD, USA. He is currently a Signal Processing Team Leader with the U.S. Army Research Laboratory, Adelphi, MD, USA, where he is involved in the research and development of several versions of ultrawideband (UWB) radar systems which have been used for proof-of-concept demonstrations in many concealed target detection programs. He has been providing synthetic aperture radar (SAR) signal-processing technical consultations to industry for the developments of many state-of-the-art UWB radars. He has been involved in development of algorithms for SAR signal and image processing. He has authored or co-authored approximately 100 conferences, journals, and technical publications. He holds nine patents and other pending patents in SAR signal processing.

Mr. Nguyen has been a member of the SPIE Technical Committee on Radar Sensor Technology since 2009. He was a recipient of the U.S. Army Research and Development Achievement Awards in 2006, 2008, and 2010, the Army Research Laboratory Award for Science in 2010, and the U.S. Army Superior Civilian Performance Award in 2011.

Petre Stoica (F'94) is a Professor of signal and system modeling with Uppsala University, Uppsala, Sweden.

Dr. Stoica is a Fellow of the European Association for Signal Processing and the Royal Statistical Society. He is a member of the Royal Swedish Academy of Engineering Sciences, the European Academy of Sciences, and the Royal Society of Sciences, a Foreign Member of the United States National Academy of Engineering, and an Honorary Member of the Romanian Academy.